Batteries & Supercaps

Research Article
doi.org/10.1002/batt.202400132

Chemistry Europe
European Chemical Societies Publishing

www.batteries-supercaps.org

Organic Mixed Ionic-Electronic Conductors as Multi-Functional Binders for Energy-Dense Carbon-Free Solid-State Batteries

Liyi Zhao,[a] Qingyu Dong,[a] Xuechun Wang,[a] Zhiyun Li,[c] Hui Shao,*[a] Yanbin Shen,*[a] and Liwei Chen[a, b]

Solid-state lithium-metal batteries are considered as one of the most promising candidates for next-generation energy storage devices with high energy density and enhanced safety. Great efforts have been made to design solid-state electrolytes with enhanced ionic conductivity and to protect the electrochemical interface of the lithium anode. However, the obstruction of ionic-electronic transport within the cathode remains as another key challenge that needs to be addressed for the practical application of solid-state batteries. Here, we prepared organic mixed ionic-electronic conductors (OMIECs) by in-situ co-polymerization of three organic monomers (boron-type cross-linker, ionic liquid, and sulfolene) in the network of poly(3,4-ethylenedioxythiophene)/poly(4-styrenesulfonate). The as-prepared OMIECs show an electronic conductivity up to 33.6 $S\,cm^{-1}$ and ionic conductivity of 1.7×10^{-4} $S\,cm^{-1}$ at 30 °C, and also binder functionality, providing a combined path for Li^+/e^- transport in cathodes and maintaining mechanical/(electro−)chemical stability. As a result, solid-state cathodes composed of 90.0 wt% active materials and only 10.0 wt% OMIECs display exceptional electrochemical characteristics at 30 °C, including high C-rate capabilities and prolonged cycle life. This novel design of all-in-one OMIECs for carbon-free cathodes demonstrates a promising strategy for developing multifunctional additives for high-performance solid-state batteries.

Introduction

Solid-state lithium-metal batteries (SSLBs) are poised to redefine the landscape of energy storage with their potential for inherently enhanced safety and superior energy density compared to conventional liquid-electrolyte-based lithium-ion batteries.[1–3] Ongoing researches within the domain of SSLBs predominantly concentrate on the development of solid-state electrolytes (SSEs) and the optimization of their interfaces with the highly reactive lithium-metal anode.[2,4] However, a critical yet often overlooked challenge in SSLBs is the facilitation of the ionic and electronic transport in electrodes, a concern that becomes particularly pronounced when evaluating thick cathodes designed for practical solid-state batteries.[5–7] In the architecture of cathodes for traditional lithium-ion batteries, the pores of the cathodes are filled with liquid electrolytes and integrated with conductive carbon to ensure ionic and electronic connectivity within the electrodes.[8,9] However, in solid-state systems, conventional electrode formulations are insufficient to provide mobile Li^+ for the redox reactions of the electroactive materials.[10] Additional ionic conductors (~20.0–30.0 wt% of the total electrode) are often introduced into cathodes to construct a Li^+ transport network.[11–13] This approach exacerbates the interface challenges and dilutes the proportion of active materials, thus impeding energy density enhancements.[14,15] Addressing the multiple issues of inadequate ionic/electronic conduction, solid-solid interfacial contacts, contacting separation during cycling, (electro−)chemical side reactions, and the low loading of active materials within solid-state cathodes requires a comprehensive reevaluation and redesign of electrode formulations.

In the quest to enhance Li^+/e^- transport within solid-state cathodes, three primary strategies have emerged as focal points of contemporary research. The first approach involves incorporating conductive additives with high Li^+/e^- conductivity into solid-state cathodes.[16–20] For example, the integration of plastic crystal or inorganic electrolytes mixed with electron conductors within solid-state cathodes to achieve optimized Li^+/e^- conductivity. However, when applied to cells designed for high energy density, featuring cathode materials with high capacity and voltage, the plastic crystal or inorganic electrolyte additives may undergo decomposition, leading to a decline in cell capacity due to the exhaustion of conductive additives after cycling processes.[21,22] A second approach is to change point

[a] Dr. L. Zhao, Dr. Q. Dong, Ms. X. Wang, Dr. H. Shao, Prof. Y. Shen, Prof. L. Chen
i-Lab, Suzhou Institute of Nano-Tech and Nano-Bionics (SINANO), Chinese Academy of Sciences (CAS), Suzhou 215123, China
E-mail: hshao2023@sinano.ac.cn
ybshen2017@sinano.ac.cn

[b] Prof. L. Chen
School of Chemistry and Chemical Engineering, Frontiers Science Center for Transformative Molecules, Shanghai Electrochemical Energy Device Research Center (SEED) and In-situ Center for Physical Sciences, Shanghai Jiao Tong University, Shanghai 200240, China

[c] Ms. Z. Li
Vacuum Interconnected Nanotech Workstation (Nano-X), Suzhou Institute of Nano-Tech and Nano-Bionics (SINANO), Chinese Academy of Sciences (CAS), Suzhou 215123, China

Supporting information for this article is available on the WWW under https://doi.org/10.1002/batt.202400132

contact to a more compliant soft contact. Since inorganic conductors are typically introduced in the form of particles, they are prone to aggregation within cathodes, compounded by the inherent challenges of solid-solid contact between inorganic conductors and active cathode materials, which escalates the energy barrier impeding Li^+/e^- transport.[23,24] To this end, the incorporation of organic conductors to realize intimate contact within solid-state cathodes is an effective method. The third approach is to reduce the types or proportions of inactive components in the solid-state cathode to minimize transport barriers.[12,25,26] For instance, the development of conducting binders presents an opportunity to circumvent the transmission limitations posed by insulating binders, thereby enhancing the proportion of active materials. However, most conducting binders still face problems of having a narrow electrochemical window and low conductivity at ambient temperature. Addressing these challenges, the construction of integrated battery cathodes that facilitates ionic-electronic interconnectivity and maintains interface stability emerges as both crucial and pressing for designing high-performance SSLBs.

An emerging category of organic mixed ionic-electronic conductors (termed OMIECs) has attracted great attention in battery systems due to their easy manufacturing, customizable design for specific applications, and long-range conductivity.[26–30] OMIECs offer the potential to substantially mitigate the resistance within the electrode, concurrently preserving the structural cohesion like the conventional binders. For instance, poly(3,4-ethylenedioxythiophene)/poly(4-styrenesulfonate) (PEDOT:PSS) is the most studied OMIECs due to its high electronic conductivity, binder functionality, and stability under ambient conditions.[27,31] However, the ionic conductivity of PEDOT:PSS is notably deficient, which significantly limits the Li-ion migration within the electrodes. Thus, the development of novel OMIECs that amalgamates electron conductivity, Li-ion conductivity, and mechanical robustness within a singular electrode additive is imperative. Such an advancement would effectively diminish the presence of inert materials and improve the ratio of active materials within the electrodes, heralding enhancements in both energy density and efficiency of battery systems.[32,33]

In this paper, we propose a novel in-situ polymerization strategy that integrates PEDOT:PSS with a polymer electrolyte to fabricate OMIECs. The OMIECs show an electronic conductivity up to 33.6 $S\,cm^{-1}$ and ionic conductivity of 1.7×10^{-4} $S\,cm^{-1}$ at 30 °C. The electrostatic interactions between the positively charged polymer electrolyte and negatively charged PEDOT:PSS produce ionic cross-links, thereby enhancing mechanical strength and improving structural stability. The designed OMIECs can minimize the quantity of ionic conductor, electronic conductor, and binder additives needed for the cathode, reduce the solid-solid contact separation, interface side reactions, and active substance proportion fundamentally, and lead to long-cycling and high-rate performance at 30 °C. As a result, a carbon-free $LiFePO_4$ (LFP) cell with 10.0 wt% OMIECs delivers a capacity of 145.0 $mAh\,g^{-1}$ at 1.0 C and a capacity retention of 80.7% after 1000 cycles. Moreover, carbon-free $LiCoO_2$ (LCO) with 10.0 wt% of OMIECs cell also exhibits excellent cycle stability with a capacity retention of 99.8% after 200 cycles at 0.2 C. Hence, the trifunctional OMIECs designed for carbon-free cathodes show promise as a robust strategy for the next generation of high-performance solid-state batteries.

Results and Discussion

Design of OMIECs

Figure 1a illustrates the trifunctionality of OMIECs (high Li^+ transport, enhanced e^- transport, and regulated viscosity) and the benefits of utilizing OMIECs for solid-state cathodes. Conventionally, a solid-state cathode requires approximately 30.0 wt% conducting additives and 10.0 wt% binders to facilitate Li^+/e^- transport connectivity and enhance the electrode structural stability. However, the introduction of inactive materials often results in extensive solid-solid point contacts, detachment at these contacts during cycling, and potential (electro−)chemical side reactions within solid-state cathodes. Such phenomena could hinder charge carrier transport and deteriorate the overall battery performance. Notably, the integration of trifunctional OMIECs, characterized by superior Li^+/e^- conductivity and modulated viscosity, enables an optimized material composition, enhanced interfacial contact, and improved conductivities within the solid-state cathode throughout repetitive discharge and charge processes. OMIECs could also mitigate the pulverization of cathode particles while maintaining Li^+/e^- accessibility, attributed to the inherent adhesive properties of OMIECs. Compared to the conventional solid-state cathode, the content of active materials of OMIECs-based cathode is improved and up to 90.0 wt% (Figure 1b), which is crucial for the development of high energy density batteries.

As one of the most studied mixed conductors, PEDOT:PSS can maintain close contact with active particles throughout the cycling process. However, the inherently lower conductivity of unmodified PEDOT:PSS requires further enhancements to improve Li^+/e^- transport, especially under high C-rate operations. To tackle this challenge, electrolyte monomers and lithium bis(tri-fuoromethanesulfonyl)imide (LiTFSI) were incorporated into PEDOT:PSS solution and then in-situ polymerized to obtain OMIECs with blend ratios ranging from 3/1 to 1/2. 2, 2-azobisisobutyronitrile (AIBN), a heat-induced radical initiator, was employed to promote the conversion of liquid monomers to polymer electrolytes (PEs) at 70 °C for 3 h. As shown in Figure 1c, this strategy effectively segregates the electron-conducting PEDOT and the lithium-ion-conducting PSS, instilling a screening effect that markedly enhances the crystallinity of PEDOT polymer. Consequently, the structural modification substantially boosts the Li^+/e^- conductivity of the OMIECs, as will be further discussed later.

Research Article
doi.org/10.1002/batt.202400132
Chemistry Europe
European Chemical Societies Publishing

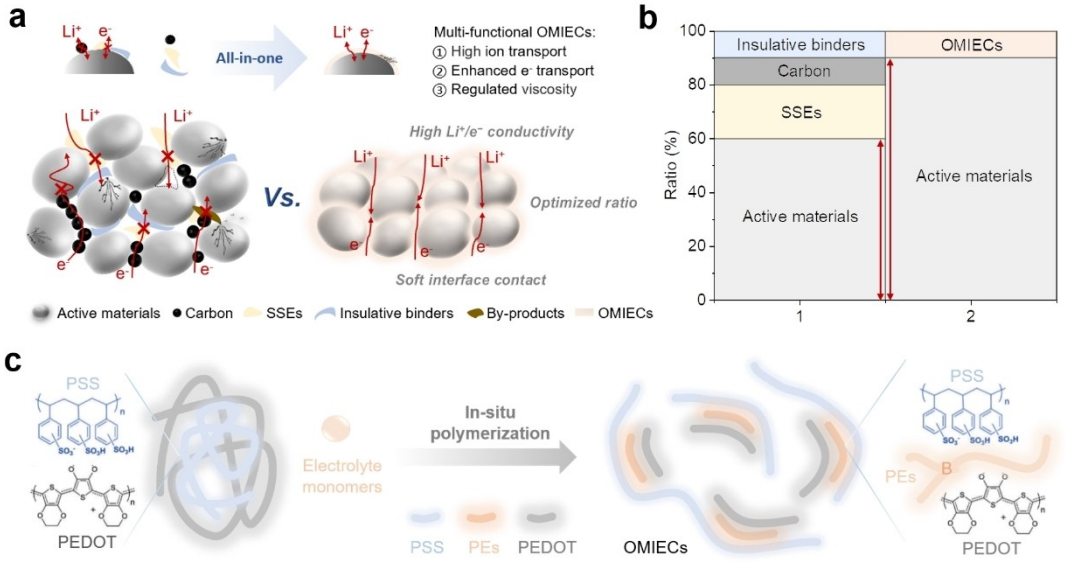

Figure 1. Design of OMIECs as multi-functional binders. a) Schematic illustration highlighting the trifunctionality of OMIECs and the advantages of utilizing OMIECs for solid-state cathodes. b) The comparison of conventional solid-state cathode and OMIECs-based cathode for the ratio of active materials. c) Proposed in-situ polymerization strategy and mechanism of PEs in PEDOT:PSS.

Characterizations of OMIECs

In our study, electrolyte monomers are polymerized within a PEDOT:PSS solution through a heat-induced free-radical reaction, resulting in the formation of OMIECs. We investigated the morphological variations between pristine PEDOT:PSS and the synthesized OMIECs. The surface of pristine PEDOT:PSS, as depicted in Figure S1a, exhibits a relatively smooth surface with some linear structures presenting an orientation of the particles which could facilitate electron transport. Similarly, the introduction of in-situ polymerized electrolytes in PEDOT:PSS solution shows well-defined pathways, likely enhancing electron transport efficiency, as shown in Figure S1b. Furthermore, the energy dispersive X-ray spectroscopy (EDS) mapping images display a uniform dispersion of C, O, S, B, N, and F atoms, suggesting a well-integrated blend of PEs and PEDOT:PSS (Figure 2a). This desirable morphology is highly beneficial for continuous Li^+/e^- transport during battery operations.

Fourier Transform Infrared Spectrometer (FTIR) spectroscopy was used to monitor the evolution of polymer monomers in PEDOT:PSS before and after polymerization (Figure 2b). Typically, polymer monomers display a characteristic C=C bond at 1640 cm^{-1}.[34,35] The disappearance of the C=C peak after polymerization evidenced the high efficiency of heat-induced polymerization in solid-state reactions. The main peaks of PEDOT:PSS appear at 1043, 1010 (–SO_3) and at 1263, 1128 and 1068 (C–O), while the $TFSI^-$ in electrolyte shows vibrations at 1403 (–SO_2 stretching), 1348 (–SO_2 stretching), 1332 (C–SO_2–N bending), 1178 (–CF_3 stretching), 1136 (C–SO_2–N bending).[36–38] It is worth noting that the intense peaks of OMIECs, which are related to the PEDOT:PSS, exhibit shifts and different relative intensities. These changes suggest an alteration around the environment of the charged PEDOT and –SO_3 group of the PSS due to the interaction with PEs.

Figure 2c presents the X-ray diffraction (XRD) patterns PEs, PEDOT:PSS, and OMIECs. The two main peaks of the OMIECs sample have sharpened after introducing polymer electrolyte into PEDOT:PSS, indicative of improved chain packing. The OMIECs show two well-defined peaks at 2Theta of 18.7° and 26.2°, corresponding respectively to the amorphous halo of PSS and the interchain planar π–π stacking distance d_{010} of PEDOT. The X-ray spectrum of OMIECs also shows a broad peak at 12.3° (d = 0.72 nm), associated with the d_{200} reflection.[39,40] Based on these data, we propose a mechanism wherein the interaction of PEDOT:PSS with Methyl sulfoxide (DMSO) initially promotes phase segregation, followed by the introduction of PEs which enhances this effect and amplifies ionic interactions within the OMIECs framework.

In addition to characterizing the morphologies and structural evolution of OMIECs binder, we evaluated the electronic conductivity of OMIECs by using a four-point probe (FPP) test and assessed the ionic conductivity by conducting the electrochemical impedance spectroscopy (EIS). When employing FPP, the ionic contribution is effectively disregarded, as the measurement predominantly captures electronic transport. Conversely, in EIS evaluations, the electronic conductivity is negligible due to its minuscule resistance impact.

The electronic conductivities of OMIECs are presented in Figure 3a. The electronic conductivity of the PEDOT:PSS, progressively increased with the incorporation of polymer electrolyte up to a ratio of 2/1, reaching the highest conductivity of 33.6 $S\,cm^{-1}$. This conductivity shows an enhancement of sevenfold compared to the pristine PEDOT:PSS film and underscores that the crystallinity of PEDOT:PSS is significantly enhanced by the presence of polymer electrolyte, leading to an increase in electronic conductivity due to the effective separation between PEDOT and PSS. The separation of PEDOT in PEDOT:PSS is attributed

Research Article
doi.org/10.1002/batt.202400132
Chemistry Europe
European Chemical Societies Publishing

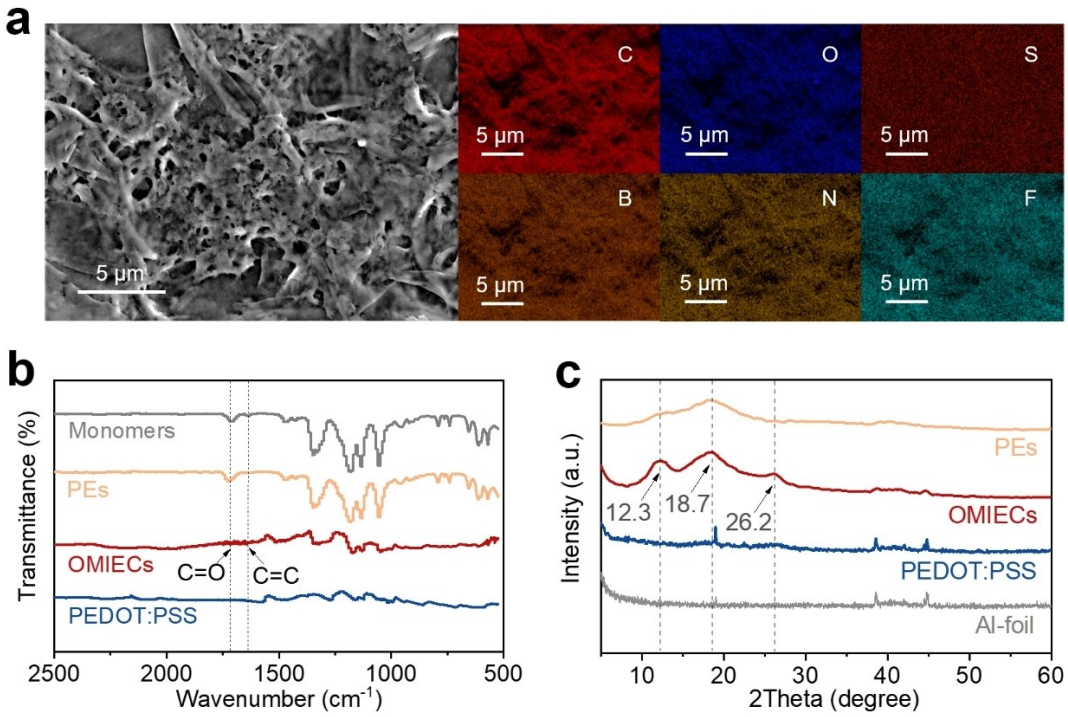

Figure 2. Morphologies and structure evaluation of OMIECs. a) SEM image of OMIECs along with corresponding EDS elemental mapping. b) FTIR spectrograms of PEDOT:PSS, electrolyte monomers, PEs, and OMIECs after in-situ polymerization. c) XRD patterns of Al foil, PEDOT:PSS, PEs, and OMIECs after polymerization.

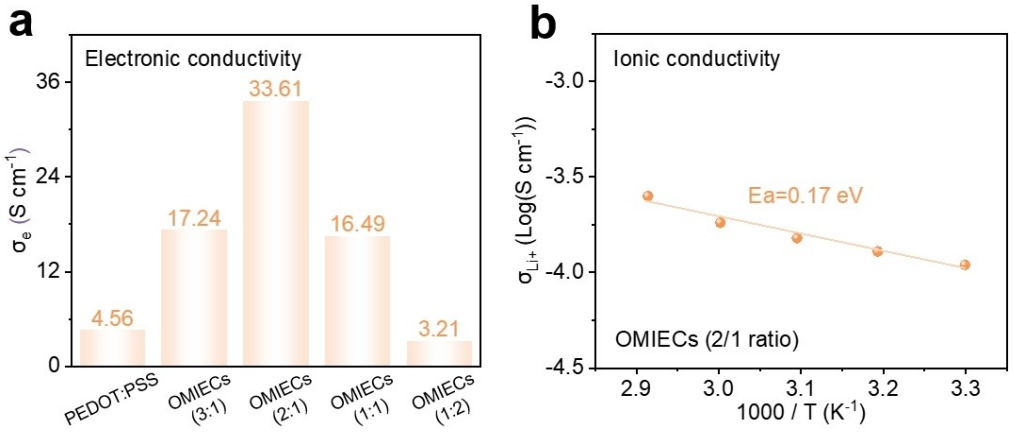

Figure 3. Electronic and ionic conductivity analysis of OMIECs. a) Electronic conductivities of PEDOT:PSS and OMIECs with 3/1, 2/1, 1/1, 1/2 ratios. b) Ionic conductivities of OMIECs (2/1 ratio) at different temperatures.

to the screening effect induced by the interaction of polymer electrolyte and PSS polymer through ion-ion interaction. This interaction separates positively charged PEDOT from negatively charged PSS polymer to form a linear conformation. Indeed, the electronic conductivities of OMIECs are significantly higher than those of the neat PEDOT:PSS suggesting a doping effect of the PEs.

The ionic conductivity of OMIECs with a polymer electrolyte ratio of 2:1 was further evaluated (Figure 3b). Typical closed semicircles of OMIECs were recorded in EIS measurements (Figure S2). The disordered PEs form an interphase with the charged polymers creating a percolating network of a highly conducting phase stabilized by interaction with PEDOT:PSS. The ionic conductivity of neat PEs is as high as 3.8×10^{-4} S cm^{-1} at 30 °C (Figure S3). The high ionic conductivity of the PEs could be attributed to its low T_g. As shown in Figure S4, the T_g of the polymer appears at −38.1 °C, indicating that the PEs may have good chain segment mobility. Also, the PEs with such low glass transition temperature can act as the "binder" in the composite electrode. When introduced the PEs in PEDOT:PSS with a ratio of 2/1, the as-prepared OMIECs sample achieves a higher ionic conductivity (1.7×10^{-4} S cm^{-1} at 30 °C) than that of PEDOT:PSS (about 10^{-7} S cm^{-1} at 30 °C). Moreover, the activation energy

Research Article
doi.org/10.1002/batt.202400132
Chemistry Europe
European Chemical Societies Publishing

(Ea) for ion mobility within the as-prepared OMIECs is remarkably low at 0.17 eV.

Cell Performance of Integrated Cathode with OMIECs

The high Li^+/e^- conductivities of the OMIECs, together with their good mechanical properties, make them good candidates to apply as conductive binders in solid-state cathode. OMIECs can cover the active particles, generating a more effective ionic and electronic contact for carbon-free cathodes. Moreover, the electrochemical window of OMIECs was measured by linear sweep voltammetry (LSV), as illustrated in Figure S5, demonstrating excellent stability till 4.7 V vs. Li^+/Li and good compatibility with a broad range of cathode active materials.

The cycling stability of OMIEC was investigated with a carbon additive-free Li | PEs | LFP@OMIECs cell at 1.0 C. As shown in Figure 4a, the OMIECs-based cell exhibited remarkable cycling stability, with an initial specific capacity of 145.0 mAh g^{-1} at 1.0 C and a capacity retention of ~80.7% after 1000 cycles, while maintaining the Coulombic efficiency close to 100.0%. Figure 4b depicts the voltage profiles at the 1st, 10th, 100th, 500th, and 1000th cycles, showing minimal polarization during the charging/discharging process and a slow capacity decay. In comparison, electrodes formulated with PVDF and PEDOT:PSS binders exhibited significant capacity degradation (Figure S6). The lower practical capacity and larger polarization of PEDOT:PSS/PVDF binders likely result from disrupted conductive pathways, impeding Li^+/e^- transport. The exceptional cycle stability of OMIECs-based electrodes can be attributed to their enhanced conductivity, improved mechanical properties, and maintained contact throughout the repeated discharge/charge processes. The specific capacities for OMIECs-based electrodes were about 3 times superior to those PEDOT:PSS-based electrodes during initial cycling. The recorded EIS spectra suggest that the overall cell resistance increases after cycles, which could result from increased interfacial resistance at long cycling (Figure 4c). Encouragingly, the resistance increases within a manageable range during the long cycles, highlighting the capability of OMIECs to sustain long cycling with high stability.

Figure 4d illustrates the rate capability of LFP cells with OMIECs binder. Upon measuring the rate capability ranging from 0.1 to 1.0 C, as expected, the highly conductive OMIECs-based LFP electrode exhibited superior electrochemical performance. The voltage profiles of OMIECs at 0.1 to 1.0 C are

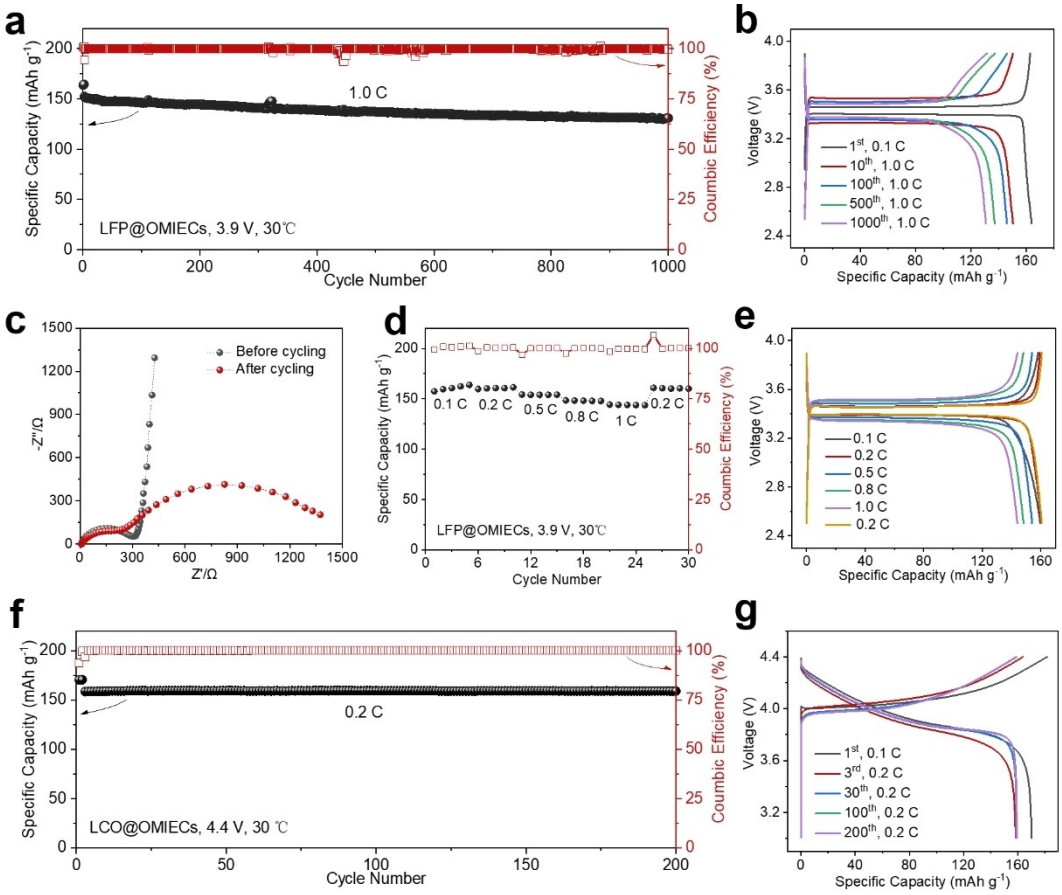

Figure 4. Cell performance of carbon-free solid-state cathodes for SSLBs. a) Long-term cycle performance of Li | PEs | LFP@OMIECs cell at 1.0 C. b) Voltage profiles of OMIECs binder in LFP carbon-free cathode for 1000 cycles at 1.0 C. c) Nyquist plots of Li | PEs | LFP@OMIECs cell before and after cycling. d) Rate capability of Li | PEs | LFP@OMIECs cell at 0.1, 0.2 0.5, 0.8, and 1.0 C. e) Voltage profiles of OMIECs binder in LFP carbon-free cathode at 0.1, 0.2 0.5, 0.8, and 1.0 C. f) Long-term cycle performance of Li | PEs | LCO@OMIECs cell at 0.2 C. g) Voltage profiles of OMIECs binder in LCO carbon-free cathode for 200 cycles at 0.2 C.

Research Article
doi.org/10.1002/batt.202400132
Chemistry Europe
European Chemical Societies Publishing

depicted in Figure 4e, where low overpotentials can be seen even at 1.0 C owing to the improved Li^+/e^- interconnection within the solid-state cathodes.

Carbon-free Li|PEs|LCO@OMIECs cell similarly demonstrates remarkable cycle stability (Figure 4f), with a capacity retention of 99.8% after 200 cycles at 0.2 C. Voltage profiles across the 1st, 3rd, 30th, 100th, and 200th cycles, shown in Figure 4g, maintain consistent shapes with minimal capacity degradation. Notably, even when the OMIECs binder was reduced to 10.0% (with LFP/LCO active materials increased to 90.0%), the electrode still displayed reliable cycle performance.

Although some binders reported in literature meet the requirements of intimate interfacial contact and electronic conductivity in solid-state cathodes, they often fall short in ionic conductivity and electrochemical stability, which can curtail cycle life and rate performance at 30 °C. OMIECs can be postulated as an ideal and stable binder with a highly promising performance which confirms its ability to behave as an outstanding electronic conducting agent and as a high Li^+ supplier for the active materials in a non-porous and carbon-free configuration.

Interface Compatibility of OMIECs-Based Cathodes

To further evaluate the effectiveness and stability of the OMIECs binder, SEM analysis was conducted to investigate the surface morphologies of the OMIECs-based cathodes before and after cycling (Figure 5a, b). The carbon-free LFP/LCO cathode with 10 wt% OMIECs showed a smooth surface morphology, uniform dispersion of the thin coating layer, and intimate contact between active materials and OMIECs binder. After 200 cycles, the LFP/LCO@OMIECs cathodes presented a surface without any cracks, demonstrating the robustness and stability of the OMIECs binder.

The active material surface compositions of the LFP@OMIECs cathode were measured by X-ray photoelectron spectroscopy (XPS). As illustrated in Figure 5c, several inorganic components derived from OMIECs decomposition were recorded, including Li_xSO_y (169.2 eV, S 2p),[41,42] Li_xNSO_y (398.8 eV, N 1 s),[43,44] and LiF (684.5 eV, F 1 s).[45–47] These findings suggest that OMIECs and their decomposition products may synergistically contribute to the formation of a uniform coating layer, thereby enhancing interfacial contact and facilitating effective transport pathways.

Conclusions

In summary, we demonstrated the in-situ polymerization synthesis of OMIECs that can serve as a trifunctional binder within solid-state cathodes. We show that the integration of OMIECs into cathode notably improves both electronic and ionic conductivity of the electrode, alongside enhancing adhesion

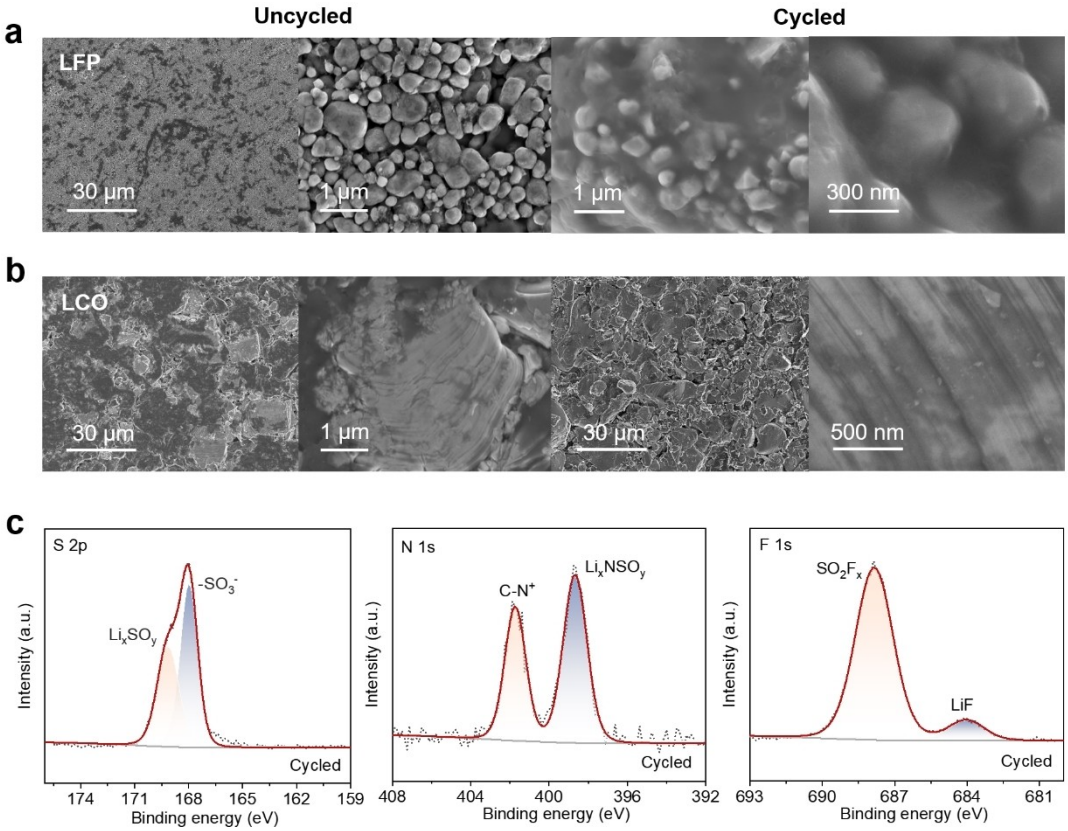

Figure 5. Interface compatibility of OMIECs-based solid-state cathodes. a) SEM images of LFP@OMIECs cathodes before and after 200 cycles. b) SEM images of LCO@OMIECs cathodes before and after 200 cycles. c) XPS spectra of LFP@OMIEC cathode after cycling (S 2p, N 1s, F 1s).

among the active materials and between the electrode composite and the current collector. Our designed OMIECs endow solid-state cathodes with temporally stable interface, structural integrity, and fast electronic/ionic transportation, contributing to an excellent cycling life and high-rate capability of SSLBs. Accordingly, carbon-free LFP@OMIECs (mass ratio = 9:1) cell achieved a capacity retention of >80.0% at 1.0 C for more than 1000 cycles. Moreover, carbon-free LCO@OMIECs (mass ratio = 9:1) cell also exhibited exceptional cycle stability with a capacity retention of 99.8% after 200 cycles at 0.2 C. This work provides the critical insight that the design of OMIECs can enhance electronic conductivity, provide high ionic transport, and are stable in a battery environment, making it an ideal choice for solid-state cathode additives.

Experimental Section

Preparation of OMIECs

Firstly, the sponge-like PEDOT:PSS particles were dissolved in anhydrous DMSO, and the solution was continuously stirred at room temperature for 24 h. Subsequently, the PEDOT:PSS solution was transferred to a reaction device in an argon-filled glove box, and the electrolyte monomers (boranetriyltris(oxy) tris(ethane-2,1-diyl) tris(2-methylacrylate),[48] 1-allyl-1-methyl-pyrrolidinium bis(trifluoromethane-sulfonyl) imide, and 3-sulfolene) and LiTFSI were introduced into the PEDOT:PSS solution. Then it was continuously stirred at 70 °C for 3 h to obtain a deep blue slurry of OMIECs by in-situ polymerization with blend ratios of 3/1, 2/1, 1/1, to 1/2. AIBN as a heat-induced radical initiator was employed to promote the conversion of liquid monomers to PEs.

Preparation of OMIECs-Based Cathode and Battery

Active materials ($LiFePO_4$ or $LiCoO_2$) were added in the deep blue slurry of OMIECs, and stirred at 60 °C for 8 h. The mass ratio of the active cathodes and OMIECs was 9:1. Then the mixed slurry was cast onto aluminum foil and dried in vacuum at 80 °C overnight to obtain a carbon-free OMIECs-based cathode (labeled as LFP@OMIECs or LCO@OMIECs). Active material loading of the OMIECs-based cathode was employed as ~3.0 mg cm^{-2} for the regular test. To prepare the PEs, boranetriyltris(oxy) tris(ethane-2,1-diyl) tris(2-methylacrylate), 1-allyl-1-methyl-pyrrolidinium bis(trifluoromethanesulfonyl) imide, 3-sulfolene, and LiTFSI were mixed at 1:7:2:2.5 mass ratio and stirred at room temperature until a transparent precursor solution was obtained. Then, photo-initiator (IRGACURE 819, 0.5% molar weight of the monomers) was added to the above transparent solution, and the mixture was stirred for about 0.5 h. Afterwards, the polymerization was initiated by ultraviolet light for 5 min to obtain the PEs. Coin 2032-type cells were assembled using LFP@OMIECs or LCO@OMIECs cathodes, PEs, and lithium metal anode inside an argon-filled glovebox.

Materials Characterization

The morphology of the OMIECs and the OMIECs-based cathodes before and after cycling were examined by scanning electron microscope (SEM) with an accelerating voltage of 10 kV equipped with energy dispersive X-ray spectrometry. Fourier transform infrared (FTIR) spectra of PEDOT:PSS, electrolyte monomers, PEs, and OMIECs were recorded using a Thermo Scientific Nicolet 6700 spectrometer with wavenumbers from 2500 to 500 cm^{-1}. The crystallinity and phase compositions of PEDOT:PSS, PEs, and OMIECs samples were investigated using X-ray diffraction (XRD) measurements on a D8 diffractometer (Bruker) with Cu Kα radiation with a scanning rate of 10° min^{-1} in the 2θ range of 5°–60°. X-ray photoelectron spectroscopy (XPS) measurements were performed by a Thermo Scientific ESCALAB Xi+ using a monochromatic Al Kα X-ray source (1486.6 eV) with a pass energy of 30 eV in a Vacuum Interconnected Nanotech Workstation (Nano-X).

Electrochemical Measurement

The electronic conductivity (σ_e) of PEDOT:PSS and OMIECs was evaluated using a four-point probe (FPP) and the ionic conductivity (σ_i) was evaluated employing an electrochemical impedance spectroscopy (EIS). EIS was conducted at a temperature range of 30 °C to 70 °C, where the frequency range was set from 100 mHz to 7 MHz with an amplitude of 10 mV. Note that we made a pre-treatment of the stainless-steel electrode with a polymer electrolyte film to block the electron transport between the steel sheet and OMIECs.[7] The thickness of the polymer electrolyte film on the steel sheet can be negligible compared to the thickness of OMIECs (>40 μm). The ionic conductivity was calculated as follows:

$$\sigma_i = L/(RS) \quad (1)$$

where L is the thickness of the OMIECs membrane, R is the resistance, and S is the effective electrode surface area.

The electrochemical stability window of OMIECs was determined by LSV from open circuit voltage to 6 V at a scan rate of 0.1 mV/s. The above tests were carried out using an electrochemical workstation (the Bio-logic VPM-300).

The cycle life and rate capability of the Li|PEs|LFP@OMIECs and Li|PEs|LCO@OMIECs cells were measured at voltage ranges of 2.5–3.9 V (LFP) and 3.0–4.4 V (LCO) at 30 °C. The electrochemical performance of the cell was tested via a Neware BTS battery tester.

Acknowledgements

This work was financially supported by the National Key R&D Program of China (2021YFB3800300), the National Natural Science Foundation of China (Grant no. 22179143, 22309201), and the Jiangsu Funding Program for Excellent Postdoctoral Talent. The authors are grateful for the technical support for Nano-X from Suzhou Institute of Nano-Tech and Nano-Bionics, Chinese Academy of Sciences (SINANO).

Conflict of Interests

The authors declare no conflict of interest.

Data Availability Statement

The data that support the findings of this study are available from the corresponding author upon reasonable request.

Keywords: Organic mixed ionic-electronic conductors · multifunctional binders · ionic-electronic interconnection · stable interface · carbon-free solid-state cathodes

[1] H. Wan, Z. Wang, W. Zhang, X. He, C. Wang, *Nature* **2023**, *623*, 739–744.
[2] Y. B. Shen, Y. T. Zhang, S. J. Han, J. W. Wang, Z. Q. Peng, L. W. Chen, *Joule* **2018**, *2*, 1674–1689.
[3] A. M. Nolan, Y. Z. Zhu, X. F. He, Q. Bai, Y. F. Mo, *Joule* **2018**, *2*, 2016–2046.
[4] S. S. Shinde, N. K. Wagh, S. H. Kim, J. H. Lee, *Adv. Sci.* **2023**, *10*, 2304235.
[5] P. Minnmann, F. Strauss, A. Bielefeld, R. Ruess, P. Adelhelm, S. Burkhardt, S. L. Dreyer, E. Trevisanello, H. Ehrenberg, T. Brezesinski, F. H. Richter, J. Janek, *Adv. Energy Mater.* **2022**, *12*, 2201425.
[6] Y. Liu, X. F. An, K. Yang, J. B. Ma, J. S. Mi, D. F. Zhang, X. Cheng, Y. H. Li, Y. T. Ma, M. Liu, F. Y. Kang, Y. B. He, *Energy Environ. Sci.* **2024**, *17*, 344–353.
[7] H. Li, F. Lian, N. Meng, C. Y. Xiong, N. Wu, B. Y. Xu, Y. T. Li, *Adv. Funct. Mater.* **2021**, *31*, 2008487.
[8] Y. T. Liu, R. H. Zhang, J. Wang, Y. Wang, *iScience* **2021**, *24*, 102332.
[9] J. G. Zheng, C. G. Sun, Z. X. Wang, S. J. Liu, B. G. An, Z. H. Sun, F. Li, *Angew. Chem. Int. Ed.* **2021**, *60*, 18448–18453.
[10] Z. Zeng, J. Cheng, Y. Y. Li, H. Q. Zhang, D. P. Li, H. B. Liu, F. J. Ji, Q. Sun, L. J. Ci, *Mat. Today Phys.* **2023**, *32*,101009.
[11] J. Li, J. Z. Qi, F. Jin, F. R. Zhang, L. Zheng, L. F. Tang, R. Huang, J. J. Xu, H. W. Chen, M. Liu, Y. J. Qiu, A. I. Cooper, Y. B. Shen, L. W. Chen, *Nat. Commun.* **2022**, *13*, 2031.
[12] Y. C. Jung, S. M. Lee, J. H. Choi, S. S. Jang, D. W. Kim, *J. Electrochem. Soc.* **2015**, *162*, A704–A710.
[13] N. C. Rosero-Navarro, A. Miura, K. Tadanaga, *J. Power Sources* **2018**, *396*, 33–40.
[14] D. Cao, Y. Zhao, X. Sun, A. Natan, Y. Wang, P. Xiang, W. Wang, H. Zhu, *ACS Energy Lett.* **2020**, *5*, 3468–3489.
[15] S. P. Culver, R. Koerver, W. G. Zeier, J. Janek, *Adv. Energy Mater.* **2019**, *9*, 1900626.
[16] C. Wang, K. R. Adair, J. Liang, X. Li, Y. Sun, X. Li, J. Wang, Q. Sun, F. Zhao, X. Lin, R. Li, H. Huang, L. Zhang, R. Yang, S. Lu, X. Sun, *Adv. Funct. Mater.* **2019**, *29*, 1900392.
[17] H. C. Gao, L. G. Xue, S. Xin, K. Park, J. B. Goodenough, *Angew. Chem. Int. Ed.* **2017**, *56*, 5541–5545.
[18] D. Zhou, Y. B. He, R. L. Liu, M. Liu, H. D. Du, B. H. Li, Q. Cai, Q. H. Yang, F. Y. Kang, *Adv. Energy Mater.* **2015**, *5*, 1500353.
[19] S. J. Chen, J. X. Zhang, L. Nie, X. C. Hu, Y. Q. Huang, Y. Yu, W. Liu, *Adv. Mater.* **2021**, *33*, 2002325.
[20] H. Erabhoina, M. Thelakkat, *Sci. Rep.-Uk* **2022**, *12*, 5454.
[21] K. Yoon, J. J. Kim, W. M. Seong, M. H. Lee, K. Kang, *Sci. Rep.-Uk* **2018**, *8*, 8066.
[22] X. F. Yan, Z. B. Li, Z. Y. Wen, W. Q. Han, *J. Phys. Chem. C* **2017**, *121*, 1431–1435.
[23] K. Kerman, A. Luntz, V. Viswanathan, Y. M. Chiang, Z. B. Chen, *J. Electrochem. Soc.* **2017**, *164*, A1731–A1744.
[24] R. C. Xu, X. H. Xia, S. H. Li, S. Z. Zhang, X. L. Wang, J. P. Tu, *J. Mater. Chem. A* **2017**, *5*, 6310–6317.
[25] D. C. Lin, W. Liu, Y. Y. Liu, H. R. Lee, P. C. Hsu, K. Liu, Y. Cui, *Nano Lett.* **2016**, *16*, 459–465.
[26] C. Ma, K. Dai, H. S. Hou, X. B. Ji, L. B. Chen, D. C. Ivey, W. F. Wei, *Adv. Sci.* **2018**, *5*, 1700996.
[27] R. del Olmo, T. C. Mendes, M. Forsyth, N. Casado, *J. Mater. Chem. A* **2022**, *10*, 19777–19786.
[28] N. J. Kong, M. S. Kim, J. H. Park, J. Kim, J. Jin, H. W. Lee, S. J. Kang, *Energy Storage Mater.* **2024**, *64*, 103074.
[29] M. Y. Jia, Z. J. Bi, X. X. Guo, *Chem. Commun.* **2022**, *58*, 8638–8641.
[30] G. Pace, A. Zele, P. Nguyen, R. J. Clement, R. A. Segalman, *Chem. Mater.* **2023**, *35*, 8101–8111.
[31] J. M. Kim, H. S. Park, J. H. Park, T. H. Kim, H. K. Song, S. Y. Lee, *ACS Appl. Mater. Interfaces* **2014**, *6*, 12789–12797.
[32] R. Q. Guo, F. Wu, X. R. Wang, Y. Bai, C. Wu, *J. Electrochem.* **2022**, *28* (12), 2219011.
[33] Y. Luo, R. Q. Ma, Z. L. Gong, Y. Yang, *J. Electrochem.* **2023**, *29* (3), 2217007.
[34] W. W. Zeng, L. Wang, X. Peng, T. F. Liu, Y. Y. Jiang, F. Qin, L. Hu, P. K. Chu, K. F. Huo, Y. H. Zhou, *Adv. Energy Mater.* **2018**, *8*, 1702314-1–1702314-8.
[35] W. Fan, T. Liu, F. Wu, S. J. Wang, S. B. Ge, Y. H. Li, J. L. Liu, H. R. Ye, R. X. Lei, C. Wang, Q. L. Che, Y. Li, *ACS Nano* **2023**, *17*, 21073–21082.
[36] L. F. Tang, B. Chen, Z. H. Zhang, C. Ma, J. C. Chen, Y. Huang, F. Zhang, Q. Y. Dong, G. Y. Xue, D. Chen, C. Hu, S. Li, Z. Liu, Y. B. Shen, Q. Chen, L. Chen, *Nat. Commun.* **2023**, *14*, 2301.
[37] Z. L. Rong, Y. Sun, M. Yang, F. Y. Cheng, W. Q. Zhang, J. Chen, *Energy Storage Mater.* **2023**, *63*, 103066.
[38] C. Mendes-Felipe, J. C. Barbosa, R. Gonçalves, D. Miranda, C. M. Costa, J. L. Vilas-Vilela, S. Lanceros-Mendez, *J. Energy Chem.* **2021**, *62*, 485–496.
[39] N. Kim, S. Kee, S. H. Lee, B. H. Lee, Y. H. Kahng, Y. R. Jo, B. J. Kim, K. Lee, *Adv. Mater.* **2014**, *26*, 2268–2272.
[40] Y. Choi, C. Yoon, M. Kim, T. D. Yang, C. Fang-Yen, R. R. Dasari, K. J. Lee, W. Choi, *Phys. Rev. Lett.* **2012**, *109*, 203901.
[41] H. Chen, A. Pei, D. C. Lin, J. Xie, A. K. Yang, J. W. Xu, K. X. Lin, J. Y. Wang, H. S. Wang, F. F. Shi, D. Boyle, Y. Cui, *Adv. Energy Mater.* **2019**, *9*, 1900858.
[42] J. Y. Wei, X. Q. Zhang, L. P. Hou, P. Shi, B. Q. Li, Y. Xiao, C. Yan, H. Yuan, J. Q. Huang, *Adv. Mater.* **2020**, *32*, 2003012.
[43] F. L. Wu, S. Fang, M. Kuenzel, A. Mullaliu, J. K. Kim, X. P. Gao, T. Diemant, G. T. Kim, S. Passerini, *Joule* **2021**, *5*, 2177–2194.
[44] S. Wan, K. M. Song, J. C. Chen, S. S. Zhao, W. T. Ma, W. H. Chen, S. M. Chen, *J. Am. Chem. Soc.* **2023**, *145*, 21661–21671.
[45] Q. Y. Dong, J. H. Wu, Y. Q. Wang, J. Z. Qi, J. Wang, J. Li, L. Y. Zhao, S. L. Hu, H. Shao, Y. B. Shen, L. W. Chen, *Energy Storage Mater.* **2023**, *63*, 103154.
[46] Q. Y. Dong, F. Guo, Z. J. Cheng, Y. Y. Mao, R. Huang, F. S. Li, H. C. Dong, Q. Y. Zhang, W. Li, H. Chen, Z. J. Luo, Y. B. Shen, X. D. Wu, L. W. Chen, *ACS Appl. Energ. Mater.* **2020**, *3*, 695–704.
[47] Y. You, H. Celio, J. Y. Li, A. Dolocan, A. Manthiram, *Angew. Chem. Int. Ed.* **2018**, *57*, 6480–6485.
[48] G. Xue, J. Li, J. Chen, D. Chen, C. Hu, L. Tang, B. Chen, R. Yi, Y. Shen, L. Chen, *Acta Phys. -Chim. Sin.* **2022**, *38 (X)*, 2205012.

Manuscript received: February 29, 2024
Revised manuscript received: May 27, 2024
Accepted manuscript online: May 31, 2024
Version of record online: July 18, 2024